Atomic-Level Active Sites of Efficient Imidazolate Frameworks-Derived Nickel Catalysts for CO_2 Reduction

Fuping Pan,[a⊥] Hanguang Zhang,[b⊥] Zhenyu Liu,[c⊥] David Cullen,[d] Kexi Liu,[c] Karren More,[d] Gang Wu,[b*] Guofeng Wang,[c*] Ying Li[a*]

[a] J. Mike Walker '66 Department of Mechanical Engineering, Texas A&M University, College Station, Texas 77843, United States

[b] Department of Chemical and Biological Engineering, University at Buffalo, The State University of New York, Buffalo, New York 14260, United States

[c] Department of Mechanical Engineering and Materials Science, University of Pittsburgh, Pittsburgh, Pennsylvania 15261, United States

[d] Materials Science and Technology Division, Oak Ridge National Laboratory, Oak Ridge, Tennessee 37831, United States

[⊥] These authors contributed equally to this work.

*Corresponding authors:

gangwu@buffalo.edu (G. Wu); guw8@pitt.edu (G. Wang); yingli@tamu.edu (Y. Li)

Abstract: Nickel and nitrogen co-doped carbon (Ni-N-C) has emerged as a promising catalyst for CO_2 reduction reaction (CO_2RR); however, the chemical nature of its active sites has remained elusive. Herein, we report the exploration of the reactivity and active sites of Ni-N-C for CO_2RR. Single atomic Ni coordinated with N confined in the carbon matrix was prepared through thermal activation of chemically Ni-doped zeolitic imidazolate frameworks (ZIF) and directly visualized by aberration-corrected scanning transmission electron microscopy. Electrochemical results show the enhanced intrinsic reactivity and selectivity of Ni−N sites for the reduction of CO_2 to CO, delivering a maximum CO Faradaic efficiency of 96% at a low overpotential of 570 mV. Density functional theory (DFT) calculations predict that the edge-located Ni-N_{2+2} sites with dangling bond-containing carbon atoms is the active site facilitating the dissociation of the C−O bond of *COOH intermediate, while the bulk-hosted Ni−N_4 is kinetically inactive. Furthermore, the high capability of the edge-located Ni−N_4 being able to thermodynamically suppress the competitive hydrogen evolution is also explained. The proposal of edge-hosed Ni−N_{2+2} site provides new insight in designing high-efficiency Ni-N-C for CO_2 reduction.

Keywords: Electrocatalysis, CO_2 reduction, single atomic catalyst, nickel, density functional theory

The heavy dependence of the present economy on fossil fuels results in ever-increasing emissions of greenhouse gaseous CO_2 into the atmosphere, causing detrimental global warming and posing

challenges in future energy. Electrochemical reduction of CO_2 is regarded as a potentially sustainable solution for both reducing CO_2 concentrations and generating value-added fuels and chemicals.[1, 2] However, this desired technology faces grand obstacles owing to the sluggish kinetics of CO_2 reduction reaction (CO_2RR), together with broad distributions of multiple products and competition over hydrogen evolution reaction (HER) in aqueous media.[3, 4] Noble metals, such as Au and Ag, are the state-of-the-art catalysts showing exceptional CO_2-to-CO selectivity;[5, 6] however, the prohibitive cost requires pursuing earth-abundant catalysts with high activity, selectivity, and stability.

Towards this goal, metal and nitrogen doped carbons (M-N-C) have gained extensive attention as cost-effective non-precious catalysts for CO_2 reduction,[7-12] in which nitrogen coordinated metal (in particular, $M{-}N_4$) was believed to be catalytic active sites owing to their optimal binding strength with the chemical species involved in CO_2RR. Previous studies have demonstrated that the transition metal Ni is more active and selective than other metals (eg., Fe, Co, Mn) for the reduction of CO_2 to CO,[9, 10, 13, 14] holding great promise of being employed in practice. More attractively, upon anchoring Ni in the form of atomically dispersed atoms, single-atom Ni could achieve maximize Ni utilization efficiency and be an ideal model catalyst to explore the intrinsically catalytic nature of Ni atoms at an atomic level due to their homogeneous structure.[13, 15, 16] However, the construction of isolated Ni to achieve enhanced performance remains a grand challenge because Ni atoms tend to aggregate during the high-temperature pyrolysis process.[15, 17] The selection of suitable host precursors to hinder Ni migration is crucial to forming isolated Ni

catalysts. Metal-organic frameworks (MOFs), typically characterized by isolated metal nodes and organic-containing linkers, have been identified to be the appropriate feedstock for the synthesis of single-atom catalysts.[18-20] Li et al., started pioneer study using a zeolitic imidazolate framework (ZIF-8) as a precursor to prepare single-atom Ni-N-C by post ionic exchange of ZIF-8 with Ni followed by high-temperature treatment. However, it showed a moderate CO selectivity of 72% at a large overpotential of 890 mV.[21] Instead of using physically doping, our recent finding demonstrated the feasibility of implementing chemical doping of ZIF-8 to synthesize atomic Fe and Co structure by in situ chemically replacing Zn atoms of Zn−N_4 coordination in ZIF-8 with metal atoms followed by thermal activation.[22-24] This Ni chemical doping approach could benefit to generating high-density Ni-N sites than the typical approach of physical Ni absorption method. Consequently, we take advantage of this advancement to synthesize single atomic Ni catalyst with mostly Ni−N_4 type sites for CO_2RR.

Regarding Ni−N_4 type sites, there have been identified to have two possible forms: either embedded at the edge (denoted as Ni−N_{2+2} type) or in the bulk (denoted as Ni−N_4 type) of the carbon matrix.[25-28] However, the catalytic CO_2RR sites between these two Ni−N_4 moieties has not been distinguished yet due to the limitations in fabricating Ni-N-C with the exclusive edge- or bulk-hosted Ni−N_4. At present, the theoretical studies have been mainly restricted to predict the thermodynamic activity of the bulk Ni−N_4 type active sites for CO_2RR,[7, 10, 29] but neglected the kinetic factor especially for C-O bond breaking process. Using density functional theory (DFT) computation, we have reported that the edge-hosted M−N_{2+2} is the more kinetically active sites in

Fe(or Co)-N-C while the bulk-hosted $M{-}N_4$ is inactive because it requires insurmountable activation energy more than 1 eV for the dissociation of key intermediate *COOH.[30] Therefore, we consider both thermodynamic and kinetic factors of CO_2RR on the edge-hosted $Ni{-}N_{2+2}$ and bulk-hosted $Ni{-}N_4$ sites in our computational study, thus providing new insights into the active sites in Ni-N-C catalysts for CO_2RR.

In this work, we carried out the investigation of reactivity and active site of Ni-N-C by combining synthesizing isolated Ni catalysts derived from imidazolate frameworks and studying their catalytic CO_2RR behaviors with theoretical DFT modeling. In specific, single atomic Ni-N-C was prepared by in situ replacing Zn in ZIF-8 with Ni atoms followed by thermal activation at 1100 ºC, and their catalytic CO_2RR activity was evaluated and compared with Ni-free ZIF-8-derived N-doped carbon (N-C) counterpart. The dissociation of $C{-}O$ bond in the COOH* intermediate was theoretically investigated on both edge- and bulk-hosted $Ni{-}N_4$ to explore active sites; we also calculated the free energy barriers for CO_2RR and HER to understand observed CO and H_2 selectivity. Hence, we established that the edge-hosted $Ni{-}N_{2+2}$ is the active site, enabling a 97% CO selectivity on our Ni-N-C catalyst.

The synthesis of the Ni-N-C catalyst is schematically depicted in **Fig. 1a**, which was realized by the high-temperature treatment of Ni chemically doped ZIF-8 (Ni-ZIF) precursors. This chemical doping strategy has the advantage of incorporating the second metal as nodes (e.g., Fe and Co) in the ZIF-8 constructed by Zn^{2+} nodes bridging 2-methyimidazole linkers,[22, 23] which can bring Ni with a strong chemical bonding between Ni and N into ZIF precursors. This strong

interaction between Ni and N in the precursors could enable the production of exclusively atomically dispersed Ni rather than Ni particles during the high-temperature treatment. In the synthesis of Ni-ZIF, the methanol solution of 2-methyilmidazole was added into the $Zn(NO_3)_2 \cdot 6H_2O$ and $Ni(NO_3)_2 \cdot 6H_2O$ dissolved in the methanol. During the growth of ZIF-8 crystals composed of Zn^{2+} with 2-methylimidazole, Ni^{2+} ions are able to partially replace Zn^{2+} ions to form Ni-ZIF crystals. The crystal structure and morphology of Ni-ZIF are similar to those of ZIF-8, showing sodalite-type crystal structure and the rhombic dodecahedron shape, as revealed by powder X-ray diffraction (PXRD, **Fig. 1b**) and scanning electron microscopy (SEM, **Fig. 1c** and Fig. S1a). This suggests that the Ni^{2+} ions coordinated with N atoms from 2-methyimidazole could present in tetrahedral structure in Ni-ZIF, and that such chemically doping Ni into ZIF-8 has no obvious influence on the crystal structure of ZIF-8, which makes Ni-ZIF could be expected to produce a similar carbon matrix to ZIF-8 used as a model catalyst to reveal the role of Ni for CO_2RR. The Ni contents can be also controlled by tuning the ratio of Ni^{2+} to Zn^{2+} in the synthesis of Ni-ZIF to study the effect of Ni content on their CO_2RR performance.

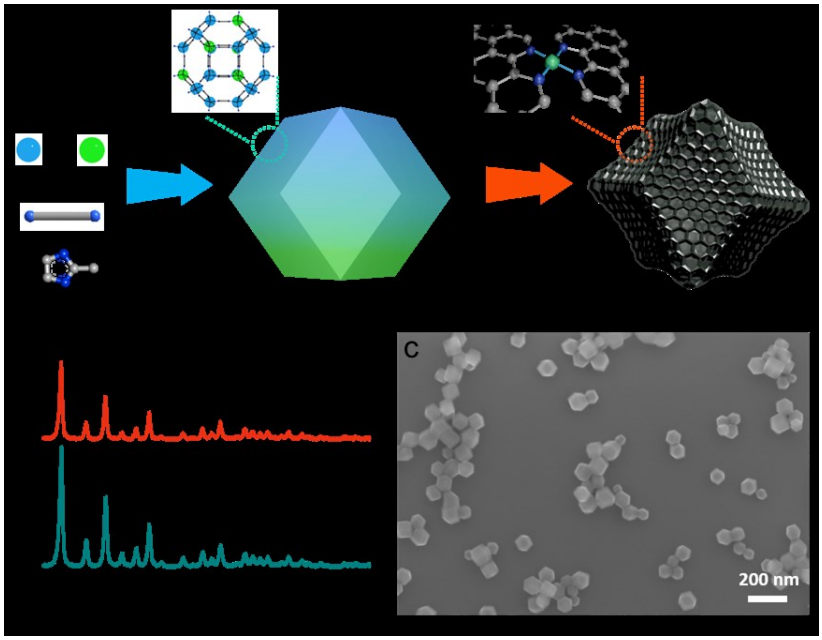

Fig. 1. (a) The schematic illustration for the preparation of Ni-N-C; (b) The patterns of PXRD for ZIF-8 and Ni-ZIF, (c) The SEM image of Ni-ZIF.

The Ni-ZIF was further converted into Ni-N-C by heating at 1100 ºC under N_2 atmosphere. During the high-temperature treatment, the Zn species are removed due to its volatile nature in the carbonization process of precursors,[31, 32] which have benefits to producing the porous structure of the carbon matrix for exposing active sites accessible for CO_2RR. It is noted that the Ni-N-C catalyst preserves the rhombic dodecahedron shape and size of particles (**Fig. 2a** and **2b**) from the Ni-ZIF precursor in a good agreement with the transformation of ZIF-8 into metal-free N-C (Fig. S1b). Ni-N-C displays two broad XRD peaks of C (002) and C (101) at 24.7º and 43.5º (**Fig. 2c**), respectively, featuring as an amorphous carbon like N-C, indicating that there is no observation of Ni metallic phases. Using the high-angle angular dark-field scanning transmission electron

microscopy (HAADF-STEM), the presence of atomically dispersed Ni atoms in the carbon matrix of Ni-N-C was directly observed in these highly bright spots as its high contrast compared to C and N atoms in the mode of HAADF-STEM (**Fig. 2d**). Especially, such Ni atoms were observed through all over the Ni-N-C catalyst with homogenous distribution, which are more likely to locate at the edges of curved carbon hexagonal planes. Furthermore, the electron energy loss spectra (EELS, **Fig. 2e**) shows the co-existence of Ni and N signals within the red circle site, while no signals can be detected in the green circle in **Fig. 2d**, which implies that the Ni atoms bond with nitrogen atoms, manifesting the formation of Ni−N coordination at edge defects of the carbon planes. As for the coordination number, our previous studies showed that Fe and Co bond with 4 N in Fe-N-C and Co-N-C prepared using the same method as to Ni-N-C.[22, 23, 30] Because the transition metals have the similar bonding characteristic to N atoms and the synthesis condition to previously reported Fe(or Co)-N-C and this work reported Ni-N-C are exactly same, it is thus more likely that Ni bonds with four N atoms forming $Ni-N_4$ embedded in the graphitic carbon matrix. In addition, other previous work also confirmed the $Ni-N_4$ structure.[11] All these characterization results demonstrate the successful synthesis of atomically dispersed Ni atoms using the effective chemically doping strategy.

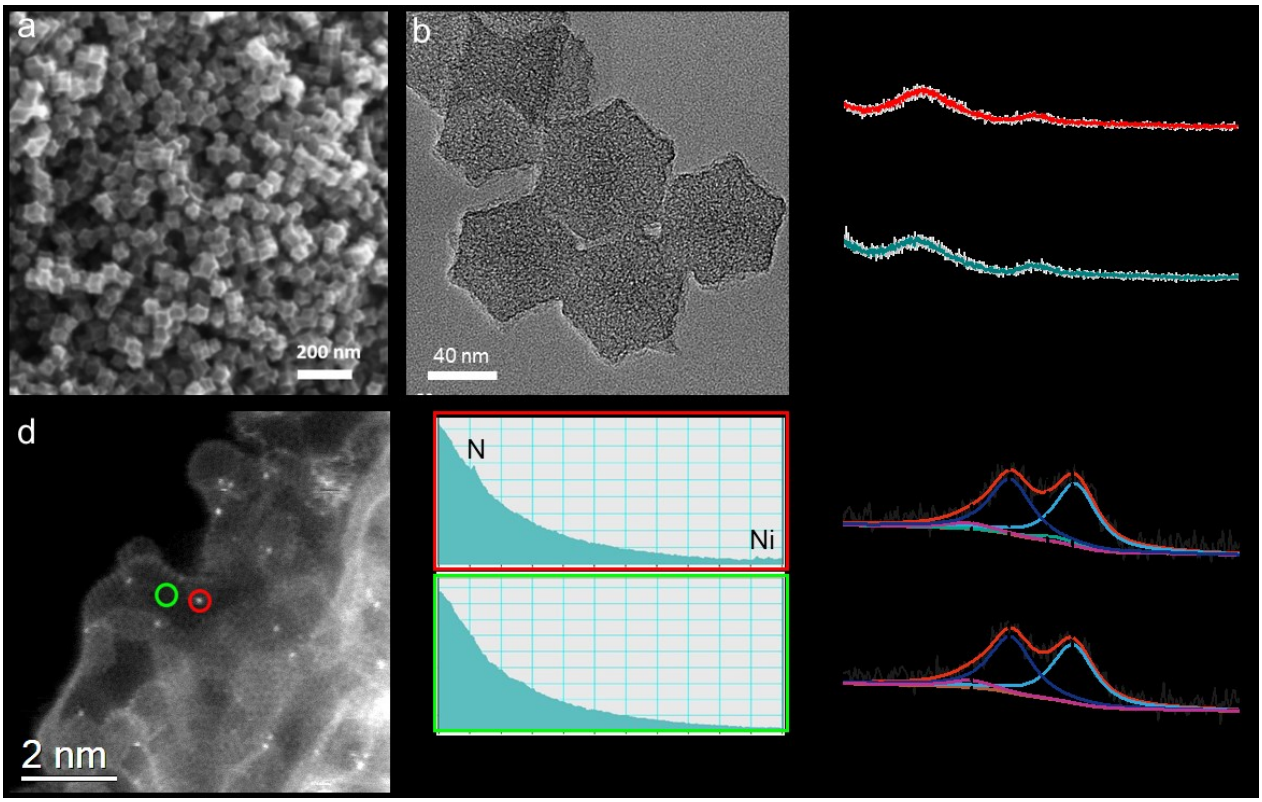

Fig. 2. (a) SEM and (b) TEM images of the Ni-N-C catalyst. (c) XRD patterns of N-C and Ni-N-C catalysts. (d) The HAADF-STEM image of the Ni-N-C catalyst associated with EELS signals (e) for the spot in the red circle with the N and Ni signals and the spot in the green circle without Ni and N signals; (f) The fitted N 1s XPS spectra N-C and Ni-N-C catalysts.

The elemental compositions and their valence states of catalysts were analyzed by X-ray photoelectron spectroscopy (XPS). Both N-C and Ni-N-C have close atomic contents of doped N (2.55 at.% in N-C and 2.92 at.% in Ni-N-C), and the Ni content is 0.16 at.% in Ni-N-C while N-C is free of Ni (Fig. S2a). The Ni−N complexes were further identified by fitting N 1s spectra (**Fig.**

2f), as revealed by the peak at the binding energy of 399.8eV, which is consistent with the typical metal-nitrogen coordination bonds in M-N-C catalysts.[22] In addition, both Ni-N-C and N-C have similar contents of pyridinic N (398.8 eV), graphitic N (401.9 eV) and oxidized N (402.5 eV),[33, 34] which allow us to minimize the difference of $N-C_X$ species in affecting CO_2 electrocatalysis performance when studying Ni-N sites. In the Ni $2p_{3/2}$ spectra, the oxidation state of Ni is close to Ni^{2+} (855.5 eV) rather than Ni^0 (852.5 eV) (Fig. S2a), suggesting the absence of metallic Ni phase in the Ni-N-C, in a good agreement with the XRD and microscopy observation. The carbon structure of the two catalysts also presents no obvious difference as revealed by Raman spectroscopy (Fig. S2b), with the same position of D band at 1348 cm^{-1} and G band at 1590 cm^{-1} as well as the similar values of I_D/I_G (0.93 for Ni-N-C and 0.94 for N-C). Therefore, the Ni-N-C catalyst with atomically dispersed Ni possesses exclusive Ni−N sites and a similar morphology and N compositions to the N-C counterpart, rendering Ni-N-C an ideal platform to elucidate the intrinsic role of Ni centers for CO_2RR.

With the successful synthesis of ZIF-derived Ni-N-C with N-C as a reference, their electrochemical activity towards CO_2 reduction was evaluated in the 0.1 M $KHCO_3$ solution. We first optimized the activity of Ni-N-C by adjusting Ni amounts used in preparing Ni-doped ZIF. As shown in Fig. S3, Ni-N-C prepared with a Ni:Zn molar ratio of 1:2 (labeled as Ni-N-C-33) exhibited the best activity, which was hence chosen to be our model Ni-N-C catalyst. **Fig. 3a** depicts linear sweep voltammetry (LSV) curves recorded in the Ar- and CO_2-saturated solution. LSV curve collected in the CO_2-saturated solution show larger currents than that obtained in the

Ar-saturated solution, indicating the occurrence of CO_2 reduction. Further comparisons demonstrate that CO_2 reduction occurs at around −0.6 V on N-C, meaning an onset overpotential of 490 mV given the equilibrium potential of CO_2/CO is −0.11 V.[35] Notably, Ni-N-C catalyzes CO_2 reduction starting at −0.4 V corresponding an onset overpotential of 290 mV, which is 200 mV smaller relative to that of N-C. The positive shift of onset potential and larger current clearly manifest that Ni−N is inherently more active toward CO_2 reduction as compared to C−N_x species.

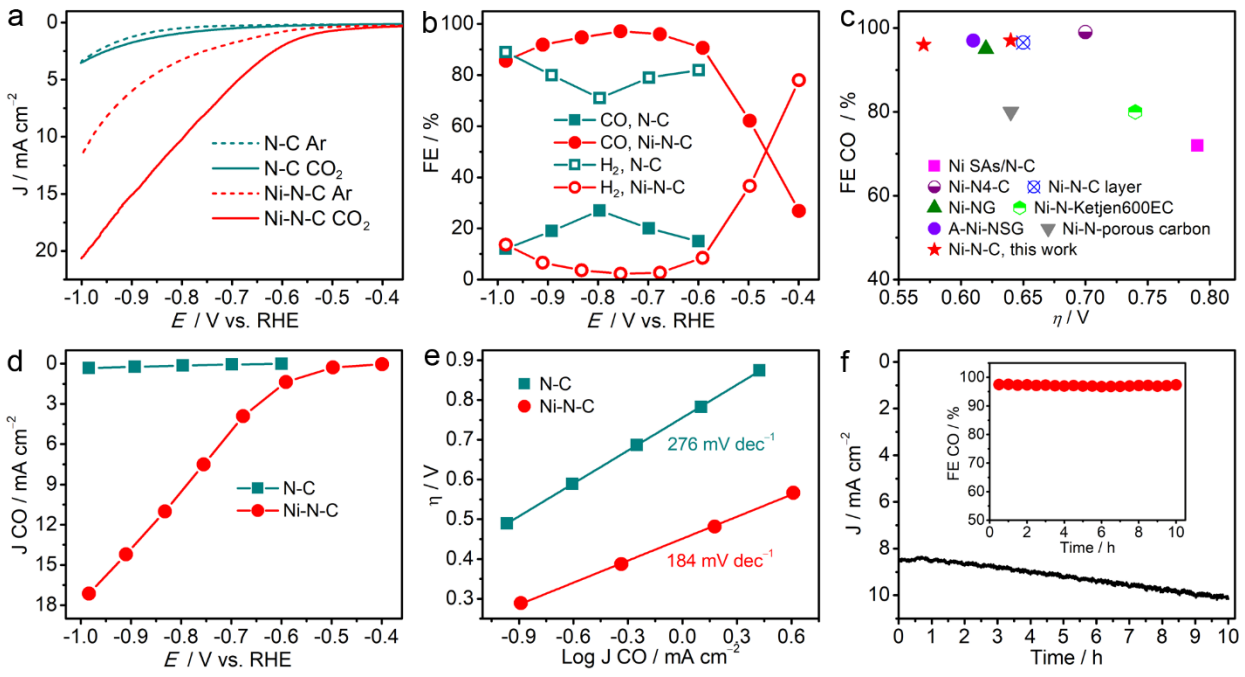

Fig. 3. (a) LSV curves in the Ar- and CO_2-saturated 0.1 M $KHCO_3$ electrolyte, (b) CO Faradaic efficiency for N-C and Ni-N-C. (d) Comparisons of maximum CO FE and corresponding overpotentials of Ni-N-C catalyst in this work with other typical Ni-based catalysts reported in the literature. Ni SAs/N-C,[21] Ni-N_4-C,[15] Ni-N-C layers,[9] Ni-NG,[13] Ni-N-Ketjen600EC,[17] A-Ni-NG,[7]

Ni-N-porous carbon.[10] (e) CO partial current density and (e) Tafel plots for N-C and Ni-N-C. (f) Current density and CO FE in a 10 h stability test.

To determine CO_2RR-generated products and their selectivity, constant-potential electrolysis was carried out. The reaction gases after stable electrolysis (Fig. S4) were vented directly into a gas chromatograph (GC) to quantitatively analyze gas-phase products; CO and H_2 were identified as the main products, accounting for total Faradaic efficiency (FE) of more than 98%. No liquid-phase products were detected by ^{1}H nuclear magnetic resonance (NMR) spectroscopy. Fig. S5 shows total current densities, in which Ni-N-C exhibited significantly larger currents than N-C, indicating higher reaction rates of Ni species. From potential-dependent CO FEs plots (**Fig. 3b**), it can be seen that N-C presented an onset CO FE of 15% at −0.60 V. The CO FE increases to a maximum value of 27% at −0.80 V and then decreases at more negative potentials. As for Ni-N-C, the onset CO FE is about 30% at −0.40 V, which quickly increases to 90% at −0.6V and to a maximum value of 97% at −0.75 V. When the potentials were swept more negatively, the CO FE decreases but still maintains a good selectivity larger than 85% even at −0.98V. These results demonstrate the higher inherent capability of Ni−N sites in selectively producing CO and suppressing HER in comparison with C−N_x. Note that maximum CO FE and current density at low overpotentials of our Ni-N-C are comparable to those of non-precious Ni-N-C catalysts reported in the literature (**Fig.3c**, Table S1).

In addition, Ni-N-C showed a CO current of 0.03 mA cm^{-2} at −0.4 V (**Fig. 3d**), which gradually increases to 7.51 mA cm^{-2} at −0.75 V and to 17.13 at −0.98 V. In contrast, the CO current on N-C is below 0.32 mA cm^{-2} at all applied potential regions. We estimated electrochemical surface areas (ECSA) by measuring double layer capacitance (C_{dl}) using cyclic voltammograms (Fig. S6a,6b). Ni-N-C exhibited a C_{dl} of 30.9 mF cm^{-2}, which is slightly larger than that of N-C (26.7 mF cm^{-2}) (Fig. S6c). To reveal the intrinsic reactivity of Ni−N species, CO partial current density was normalized to C_{dl}. As depicted in Fig. S6d, the significant larger C_{dl}-normalized CO currents observed on Ni-N-C further evidences the enhanced reactivity of single Ni atoms as compared to Ni-free N−Cx. Although same trace amounts of Zn could remain in both Ni-N-C and N-C catalysts, the poor performance of N-C for CO_2RR indicates that such Zn residues contribute insignificantly to the observed CO_2RR activity of Ni-N-C catalyst.

We further analyzed Tafel plots to gain insights into reaction kinetics. As shown in **Fig. 3e**, Ni-N-C had a Tafel slope of 184 mV dec^{-1}, lower in comparison to 276 mV dec^{-1} of N-C. The decreased Tafel slope implies that a much faster increment of CO_2 reduction rate with increasing overpotential on Ni-N-C. Furthermore, we performed electrochemical impedance spectroscopy (EIS) tests at −0.75 V to measure charge transfer resistance (Rct) that is correlated to the electrons transferred from the catalyst surface to the reactant as well as intermediate formation inside the double layer.[36, 37] Compared to the Rct of 652.4 Ω for N-C (Fig. S7), Ni-N-C shows a lower Rct of 18.1 Ω, suggesting that Ni−N species drastically boost electron transfer and contributes to the

accelerated kinetics. Finally, the stability was examined, and Ni-N-C did not show any decay in currents and CO FEs (**Fig. 3f**), yielding a total CO amount of 1.68 mmol cm^{-2} in 10 h (Fig. S8).

To understand the observed activity and selectivity of the Ni-N-C catalyst for CO_2RR, we have performed the first-principles DFT calculations to predict the thermodynamics of CO_2 reduction reaction to CO on two types of Ni−N_4 sites (Fig. S9). In our previous study, we computationally studied the CO_2RR on the bulk-hosted Fe−N_4 moiety embedded in a graphitic layer (denoted as M−N_4−C_{10}) and the edge-hosted M−N_{2+2} moiety bridging two adjacent armchair-like graphitic edges (denoted as M−N_{2+2}−C_8) for Fe-N-C and Co-N-C catalysts.[30] We found that M−N_{2+2}-C_8 site containing adjacent active carbon atoms with dangling bonds plays key roles in the COOH dissociation. In addition, we have experimentally demonstrated that both Fe−N_4 + Fe−N_{2+2} exist in Fe-N-C prepared by thermal activation of Fe-doped ZIF-8,[22, 38] both of which have also been confirmed by other works.[39, 40] In the current work, we used the same synthesis approach to doping Ni into ZIF-8 and convert the Ni-ZIF precursor into Ni-N-C at the same temperature without any metallic phase. This gives Ni-N-C the similar nitrogen doped carbon matrix to Fe-N-C catalysts, suggesting that the Ni^{2+} atoms most likely locate both in the basal plane of carbon and at the edge of two opposed graphene planes. We thus investigated both Ni−N_4−C_{10} and Ni−N_{2+2}−C_8 as possible active sites in DFT calculations.

We first examined the reaction heat for the dissociation reaction step of COOH* → CO* + OH*, through which one C−O bond is broken up on these two sites. Generally, there are two possible ways for *COOH bond to be dissociated. One is through the solvation of OH in electrolytes and

the other one is through adsorption of OH on the active sites. Based on the previous report,[41] OH^- is more favorable for adsorption on carbon in aqueous solution, as compared to the relatively weak solvation process. Therefore, the co-adsorption of *CO and *OH model would give a higher rate for CO_2 reduction reaction and be used in our DFT modeling. The later desorption of *CO results in gaseous CO and the hydrogenation of *OH yield aqueous H_2O as the final product. As plotted in **Fig. 4a**, the initial state of this elementary step is COOH adsorbed on the central Ni atom whereas the final state is that CO is adsorbed on Ni and OH adsorbed on an adjacent C atom after cleavage of the C−O bond. The DFT results show that this COOH dissociation step is an endothermic process requiring more than 1 eV external heat on Ni−N_4-C_{10} whereas is a desirable exothermic process on Ni−N_{2+2}-C_8 liberating more than 1 eV heat (Table S2). These results indicate that it must require insurmountable activation energy for the COOH dissociation on Ni−N_4-C_{10} sites but might require reasonable activation energy on Ni−N_{2+2}-C_8 sites. This agrees with our previous finding in Fe-N-C and Co-N-C that the carbon atoms with dangling bonds serve as active sites in the COOH dissociation.[30] Moreover, our computational results show that even if some edge carbon atoms with dangling bonds are passivated by H termination, the pathway for CO_2 reduction to CO is still thermodynamically favorable on this active site (Fig. S10 and S11). However, fully passivation of all the edge carbon atoms would break the Ni−N_{2+2} structure when CO molecule is adsorbed on this active site (Fig. S12). Therefore, we conclude that only the Ni−N_{2+2}−C_8 site having active carbon atoms with dangling bonds is thermodynamically and kinetically active for the CO_2RR.

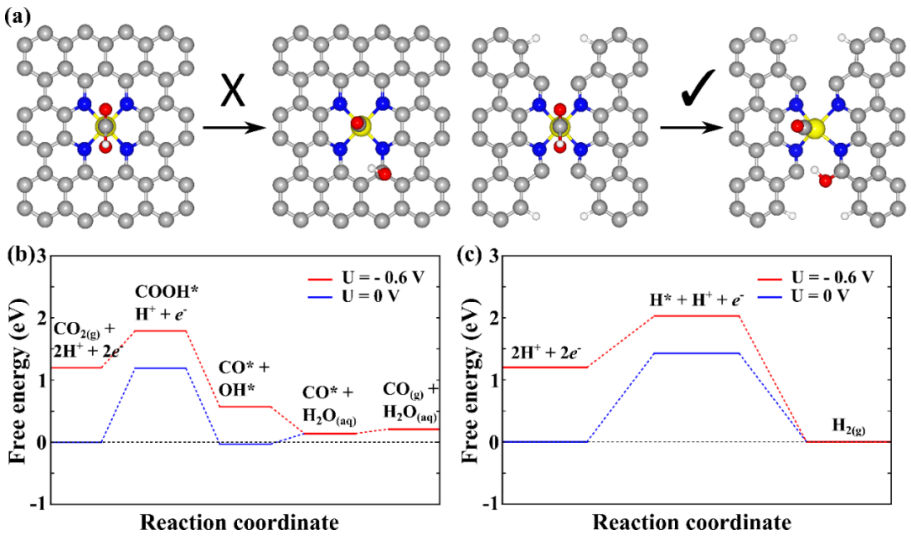

Fig. 4. (a) The initial and final state for the COOH dissociation reaction on Ni−N_4-C_{10} and Ni−N_{2+2}-C_8 sites. Calculated free energy evolution of (b) CO_2 reduction to CO, and (c) hydrogen evolution reaction on Ni−N_{2+2}-C_8 sites under applied electrode potential (U) of 0 V and −0.6 V. In the figure, the gray, blue, yellow, red, and white balls represent C, N, Ni, O, and H atoms, respectively.

Furthermore, we calculated the free energy evolution of the full pathway of CO_2 reduction to CO and the hydrogen evolution on Ni−N_{2+2}-C_8. It was found that it requires a high free energy increase of 1.19 eV from CO_2 gas phase transition to COOH* adsorbed on Ni−N_{2+2}-C_8 under an electrode potential (U) of 0 V (**Fig. 4b**). With a further decrease of U, the free energy of the elemental step of CO_2(g) to COOH* could be appreciably reduced to 0.59 eV under an electrode potential (U) of −0.6 V, as shown in **Fig. 4b**, and hence, the CO_2RR can start to proceed gradually on the Ni−N_{2+2}-C_8 sites. After the COOH bond dissociation, the CO molecule would be easily

released due to its weak binding on the active site, thus suppressing the further reduction of CO to other products. In contrast, the Volmer step for HER is predicted to be the potential-limiting step requiring the free energy increase of 1.43 and 0.75 eV at 0 and −0.6 V (**Fig. 4c**), respectively, which are larger than those of the potential-limiting step for CO_2RR on Ni−N_{2+2}-C_8 site, well explaining the observed high selectivity of Ni−N_4-C catalysts for CO generation during the CO_2RR because of the thermodynamic suppress of HER. In addition, we noted that the onset potential predicted from DFT has largely deviated with experimental results (**Fig. 3a**, Table S2), which is probably because that the definition of onset potential in DFT and experiments are different. The onset potential from DFT is the applied electrode potential at which the Gibbs free energies of all the elementary steps become negative following the pathway of CO_2RR. It should be mentioned that activation energies associated with the chemical reaction, mass diffusion, and electron transfer were not considered in DFT calculation. In contrast, the experimental onset potential is defined as the potential at which a sharp increase in reduction current is observed and thus containing kinetic effects. It is thus clear that the theoretical onset potential is not exact the onset potential from the electrochemical measurements, mainly differing in the kinetic effects. However, the trend of DFT results matches well with our experimental results.

There are some previous reports suggesting that the active site of Ni-N-C may be NiN@DV.[13, 42] We here also performed DFT calculations to examine the CO_2RR and HER on this NiN@DV site, particularly we have investigated various adsorption configurations of poisoning H atom on this site (Fig. S13). The free energy of H* adsorbed on N is calculated to be 0.67 eV, comparable

to the value 0.53 eV reported in the literature.[13, 42] However, our DFT result shows that the H* adsorbed on the activated carbon adjacent to Ni is thermodynamically more favorable (ΔG = -0.65 eV) (Fig. S14). Therefore, this adsorbed H* on the activated carbon would not be easily released and form H_2, and would, therefore, poison the NiN@DV active site. Moreover, the formation energy for NiN@DV site is always higher than that for the Ni-N_4 sites. Consequently, we conclude that NiN@DV is may not be an effective, stable active site for CO_2RR with high performance.

In addition to Ni-N-C, Fe-N-C and Co-N-C have also been widely studied for electrocatalytic CO_2 reduction to CO. Here, we summarized the intrinsically catalytic behaviors of Fe, Co, and Ni in M-N-C towards CO_2RR by comparing their catalytic performance. Our previous experimental results demonstrated that Fe-N-C and Co-N-C, prepared using the same method as to Ni-N-C reported in this work, showed onset overpotentials/maximum FEs of 0.1 V/93% and 0.27 V/45%, respectively (Fig. S15).[30] It is thus concluded that Ni-N-C has the highest CO FE (97%) but needs relatively larger onset overpotentials (−0.4 V) as compared to Fe-N-C and Co-N-C. Furthermore, the DFT-predicted onset overpotentials are −0.07 V and −0.52 V on Fe−N_{2+2}-C_8 and Co−N_{2+2}-C_8, respectively,[30] which are smaller than that of −1.19 V on Ni−N_{2+2}-C_8. The DFT calculation also confirmed the high selectivity of CO evolution on Fe−N_{2+2}-C_8 and Ni-N_{2+2}-C_8, while there exists the strong competition between HER and CO_2RR on Co−N_{2+2}-C_8 leading to poor CO FE of Co-N-C. Note that the onset potentials and CO selectivity predicted from DFT calculation are in consistent the trend of the experimental results. Furthermore, the partial current results demonstrate that Ni-N-C had smaller currents than Fe-N-C at low overpotentials but higher current

at larger overpotentials (Fig. S15), both of which are significantly larger than that of Co-N-C. Our findings agree well with other previous results that Ni-N-C and Fe-N-C holds greater promise to be used as high-efficiency and low-cost catalysts for electrocatalytic reduction of CO_2 to CO.[9, 11]

In summary, we have prepared single atomic Ni-N-C catalysts from zeolitic imidazolate frameworks for electrochemical CO_2 reduction. The atomic-level N coordinated Ni site was visualized by aberration-corrected scanning transmission electron microscopy. The resultant Ni-N-C exhibited stable CO Faradaic efficiency of 96% at a low overpotential of 570 mV, standing out among reported Ni-N-C catalysts. Further, the edge-hosted $Ni{-}N_{2+2}$-C_8 with active C atoms having dangling bonds was computationally identified to be the active moiety in terms of lower activation energy in the dissociation of COOH* intermediate while the traditionally proposed bulk-hosted $Ni{-}N_4$-C_{10} site embedded compactly in a graphitic layer is likely not active. The $Ni{-}N_{2+2}$-C_8 also showed a good capability in suppressing the competitive hydrogen evolution reaction. The identification of active $Ni{-}N_{2+2}$-C_8 containing carbon atoms with dangling bonds will provide guidelines on the design of advanced Ni-N-C catalysts for realizing an efficient and cost-effective electrochemical CO_2-to-fuels process.

Conflicts of interest

There are no conflicts to declare.

Acknowledgments

Y. Li, G. Wang, and G. Wu acknowledge the support for a collaborative project from U.S. National Science Foundation (NSF CBET #1805132, #1804534, and #1804326). G. Wang gratefully acknowledges the computational resources provided by the University of Pittsburgh Center for Research Computing as well as the Extreme Science and Engineering Discovery Environment (XSEDE), which is supported by National Science Foundation grant number ACI-1053575.

Notes and references

1. J. M. Spurgeon and B. Kumar, *Energy Environ. Sci.*, 2018, **11**, 1536-1551.
2. K. P. Kuhl, E. R. Cave, D. N. Abram and T. F. Jaramillo, *Energy & Environmental Science*, 2012, **5**, 7050-7059.
3. Z. W. Seh, J. Kibsgaard, C. F. Dickens, I. Chorkendorff, J. K. Nørskov and T. F. Jaramillo, *Science*, 2017, **355**, 1-12.
4. D. D. Zhu, J. L. Liu and S. Z. Qiao, *Adv Mater*, 2016, **28**, 3423-3452.
5. Y. Chen, C. W. Li and M. W. Kanan, *J Am Chem Soc*, 2012, **134**, 19969-19972.
6. Q. Lu, J. Rosen, Y. Zhou, G. S. Hutchings, Y. C. Kimmel, J. G. Chen and F. Jiao, *Nat. Commun.*, 2014, **5**, 3242.
7. H. B. Yang, S.-F. Hung, S. Liu, K. Yuan, S. Miao, L. Zhang, X. Huang, H.-Y. Wang, W. Cai, R. Chen, J. Gao, X. Yang, W. Chen, Y. Huang, H. M. Chen, C. M. Li, T. Zhang and B. Liu, *Nature Energy*, 2018, **3**, 140-147.
8. A. S. Varela, N. Ranjbar Sahraie, J. Steinberg, W. Ju, H.-S. Oh and P. Strasser, *Angewandte Chemie*, 2015, **127**, 10908-10912.
9. F. Pan, W. Deng, C. Justiniano and Y. Li, *Appl. Catal. B: Environ.*, 2018, **226**, 463-472.
10. W. Ju, A. Bagger, G.-P. Hao, A. S. Varela, I. Sinev, V. Bon, B. Roldan Cuenya, S. Kaskel, J. Rossmeisl and P. Strasser, *Nature Communications*, 2017, **8**, 944.
11. W. Bi, X. Li, R. You, M. Chen, R. Yuan, W. Huang, X. Wu, W. Chu, C. Wu and Y. Xie, *Adv Mater*, 2018, **30**, 1706617.
12. F. Pan, H. Zhao, W. Deng, X. Feng and Y. Li, *Electrochim Acta*, 2018, **273**, 154-161.
13. K. Jiang, S. Siahrostami, T. Zheng, Y. Hu, S. Hwang, E. Stavitski, Y. Peng, J. Dynes, M. Gangisetty, D. Su, K. Attenkofer and H. Wang, *Energy & Environmental Science*, 2018, **11**, 893-903
14. F. Pan, A. Liang, Y. Duan, Q. Liu, J. Zhang and Y. Li, *J. Mater. Chem. A* 2017, **5**, 13104-13111.
15. X. Li, W. Bi, M. Chen, Y. Sun, H. Ju, W. Yan, J. Zhu, X. Wu, W. Chu, C. Wu and Y. Xie, *J Am Chem Soc*, 2017, **139**, 14889-14892.
16. X. Cui, W. Li, P. Ryabchuk, K. Junge and M. Beller, *Nature Catalysis*, 2018, **1**, 385-397.
17. T. Moeller, W. Ju, A. Bagger, X. Wang, F. Luo, T. N. Thanh, A. Varela, J. Rossmeisl and P. Strasser, *Energy & Environmental Science*, 2019, **12**, 640-647.
18. Y. Chen, S. Ji, Y. Wang, J. Dong, W. Chen, Z. Li, R. Shen, L. Zheng, Z. Zhuang, D. Wang and Y. Li, *Angewandte Chemie International Edition*, 2017, **56**, 1-6.
19. Z. Geng, Y. Liu, X. Kong, P. Li, K. Li, Z. Liu, J. Du, M. Shu, R. Si and J. Zeng, *Adv Mater*, 2018, **30**, 1803498.

20. F. Xinzuo, S. Qichao, W. Yu, J. Long, Y. Tao, L. Yafei, Z. Qun, L. Yi and J. Hai‐Long, *Adv Mater*, 2018, **30**, 1705112.
21. C. Zhao, X. Dai, T. Yao, W. Chen, X. Wang, J. Wang, J. Yang, S. Wei, Y. Wu and Y. Li, *J Am Chem Soc*, 2017, **139**, 8078-8081.
22. H. Zhang, S. Hwang, M. Wang, Z. Feng, S. Karakalos, L. Luo, Z. Qiao, X. Xie, C. Wang, D. Su, Y. Shao and G. Wu, *J Am Chem Soc*, 2017, **139**, 14143-14149.
23. X. X. Wang, D. A. Cullen, Y.-T. Pan, S. Hwang, M. Wang, Z. Feng, J. Wang, M. H. Engelhard, H. Zhang, Y. He, Y. Shao, D. Su, K. L. More, J. S. Spendelow and G. Wu, *Adv Mater*, 2018, **30**, 1706758.
24. Y. He, S. Hwang, D. A. Cullen, M. A. Uddin, L. Langhorst, B. Li, S. Karakalos, A. J. Kropf, E. C. Wegener, J. Sokolowski, M. Chen, D. J. Myers, D. Su, K. L. More, G. Wang, S. Litster and G. Wu, *Energy & Environmental Science*, 2019, **12**, 250-260
25. A. Zitolo, V. Goellner, V. Armel, M.-T. Sougrati, T. Mineva, L. Stievano, E. Fonda and F. Jaouen, *Nat Mater*, 2015, **14**, 937-942.
26. H. T. Chung, D. A. Cullen, D. Higgins, B. T. Sneed, E. F. Holby, K. L. More and P. Zelenay, *Science*, 2017, **357**, 479-484.
27. M. Lefèvre, E. Proietti, F. Jaouen and J. P. Dodelet, *Science*, 2009, **324**, 71-74.
28. K. Liu, G. Wu and G. Wang, *The Journal of Physical Chemistry C*, 2017, **121**, 11319-11324.
29. C. Yan, H. Li, Y. Ye, H. Wu, F. Cai, R. Si, J. Xiao, S. Miao, S. Xie, F. Yang, Y. Li, G. Wang and X. Bao, *Energy & Environmental Science*, 2018, **11**, 1204-1210
30. F. Pan, H. Zhang, K. Liu, D. A. Cullen, K. L. More, M. Wang, Z. Feng, G. Wang, G. Wu and Y. Li, *ACS Catalysis*, 2018, **8**, 3116-3122.
31. B. Liu, H. Shioyama, T. Akita and Q. Xu, *J Am Chem Soc*, 2008, **130**, 5390-5391.
32. Y. Z. Chen, C. Wang, Z. Y. Wu, Y. Xiong, Q. Xu, S. H. Yu and H. L. Jiang, *Adv Mater*, 2015, **27**, 5010-5016.
33. F. Pan, B. Li, X. Xiang, G. Wang and Y. Li, *ACS Catalysis*, 2019, **9**, 2124-2133.
34. F. Pan, B. Li, W. Deng, Z. Du, Y. Gang, G. Wang and Y. Li, *Applied Catalysis B: Environmental*, 2019, **252**, 240-249.
35. M. Asadi, B. Kumar, A. Behranginia, B. A. Rosen, A. Baskin, N. Repnin, D. Pisasale, P. Phillips, W. Zhu, R. Haasch, R. F. Klie, P. Král, J. Abiade and A. Salehi-Khojin, *Nat Commun*, 2014, **5**, 4470.
36. Y. Tan, P. Liu, L. Chen, W. Cong, Y. Ito, J. Han, X. Guo, Z. Tang, T. Fujita, A. Hirata and M. W. Chen, *Adv Mater*, 2014, **26**, 8023-8028.
37. M. Asadi, K. Kim, C. Liu, A. V. Addepalli, P. Abbasi, P. Yasaei, P. Phillips, A. Behranginia, J. M. Cerrato, R. Haasch, P. Zapol, B. Kumar, R. F. Klie, J. Abiade, L. A. Curtiss and A. Salehi-Khojin, *Science*, 2016, **353**, 467-470.
38. H. Zhang, H. T. Chung, D. A. Cullen, S. Wagner, U. I. Kramm, K. L. More, P. Zelenay and G. Wu, *Energy & Environmental Science*, 2019, **12**, 2548-2558.
39. U. I. Kramm, J. Herranz, N. Larouche, T. M. Arruda, M. Lefevre, F. Jaouen, P. Bogdanoff, S. Fiechter, I. Abs-Wurmbach, S. Mukerjee and J.-P. Dodelet, *Phys Chem Chem Phys*, 2012, **14**, 11673-11688.
40. C. E. Szakacs, M. Lefevre, U. I. Kramm, J.-P. Dodelet and F. Vidal, *Phys Chem Chem Phys*, 2014, **16**, 13654-13661.
41. A. Politano and G. Chiarello, *The Journal of Chemical Physics*, 2013, **139**, 064704.
42. K. Jiang, S. Siahrostami, A. J. Akey, Y. Li, Z. Lu, J. Lattimer, Y. Hu, C. Stokes, M. Gangishetty, G. Chen, Y. Zhou, W. Hill, W.-B. Cai, D. Bell, K. Chan, J. K. Nørskov, Y. Cui and H. Wang, *Chem*, 2017, **3**, 950-960.

TOC Graphic